Engraftment of nonintegrating neural stem cells differentially perturbs cortical activity in a dose-dependent manner

Tanya N Weerakkody[1,2,5], Tapan P Patel[4], Cuiyong Yue[1], Hajime Takano[1,2], Hayley C Anderson[1], David F Meaney[4], Douglas A Coulter[1–3] and John H Wolfe[1,2,5]

[1]Research Institute of the Children's Hospital of Philadelphia, Philadelphia, PA, USA; [2]Department of Pediatrics, Perelman School of Medicine, University of Pennsylvania, Philadelphia, PA, USA; [3]Department of Neuroscience, Perelman School of Medicine, University of Pennsylvania, Philadelphia, PA, USA; [4]Department of Bioengineering, School of Engineering and Applied Sciences, University of Pennsylvania, Philadelphia, PA, USA; [5]W.F. Goodman Center for Comparative Medical Genetics, School of Veterinary Medicine, University of Pennsylvania, Philadelphia, PA, USA

Neural stem cell (NSC) therapy represents a potentially powerful approach for gene transfer in the diseased central nervous system. However, transplanted primary, embryonic stem cell- and induced pluripotent stem cell-derived NSCs generate largely undifferentiated progeny. Understanding how physiologically immature cells influence host activity is critical to evaluating the therapeutic utility of NSCs. Earlier inquiries were limited to single-cell recordings and did not address the emergent properties of neuronal ensembles. To interrogate cortical networks post-transplant, we used voltage sensitive dye imaging in mouse neocortical brain slices, which permits high temporal resolution analysis of neural activity. Although moderate NSC engraftment largely preserved host physiology, subtle defects in the activation properties of synaptic inputs were induced. High-density engraftment severely dampened cortical excitability, markedly reducing the amplitude, spatial extent, and velocity of propagating synaptic potentials in layers 2–6. These global effects may be mediated by specific disruptions in excitatory network structure in deep layers. We propose that depletion of endogenous cells in engrafted neocortex contributes to circuit alterations. Our data provide the first evidence that nonintegrating cells cause differential host impairment as a function of engrafted load. Moreover, they emphasize the necessity for efficient differentiation methods and proper controls for engraftment effects that interfere with the benefits of NSC therapy.

Received 18 February 2013; accepted 28 June 2013; advance online publication 6 August 2013. doi:10.1038/mt.2013.163

INTRODUCTION

Neural stem cells (NSCs) are promising candidates to treat a number of neurodegenerative diseases, as reviewed in 1. Such neurological disorders have been refractory to therapy due to their ubiquitous pathology. NSCs possess an inherent ability to self-renew and migrate to multifocal lesions, circumventing limitations of other gene delivery vehicles.[2] However, primary NSC transplants, as well as NSCs derived from embryonic stem cells and induced pluripotent stem cells generate a high proportion of cells that do not show evidence of neuronal differentiation or synaptic integration.[3–8] Therefore, it is important to understand whether undifferentiated or nonintegrating donor cells influence host circuit activity and if these cells cause unintended neurological impairment.

Neurophysiological data from previous transplantation studies exclusively characterized single-cell dynamics and did not assess the emergent properties of neuronal ensembles.[7,9–12] The neocortex, which largely mediates cognitive processes, is composed of interacting laminar and columnar circuits.[13] Due to its stereotypic connectivity, the cortex is an amenable system to define host circuit properties and identify abnormalities induced by exogenous cells. Voltage sensitive dye (VSD) imaging directly measures the spatiotemporal dynamics of neural networks, including the functional connectivity of the neurons involved, with high temporal resolution.[14–16] Furthermore, since VSD signals reflect membrane depolarization, subthreshold synaptic connections between functionally related areas that are difficult to detect with conventional electrophysiology can be visualized.

In this study, we used VSD imaging to test the functional impact of physiologically immature, nonintegrating donor cells in the cerebral cortex. For donor NSCs, we selected the well-established clonal line C17.2[17] that is refractory to differentiation in the cortex.[18] In contrast to primary[8,19] and immortalized NSC transplants[20,21] that show limited distribution, C17.2 cells yield high-density, titratable levels of engraftment. This system provides an ideal, testable model to evaluate the limits of physiological tolerance of host circuits to donor cells, without confounding contributions from ectopic neurons and glia. Here, we provide the first direct evidence that exogenous NSCs can disrupt neural network activity. While moderate NSC levels largely preserved physiological function, high levels severely dampened cortical activity

Correspondence: *John H Wolfe, Children's Hospital of Philadelphia, Abramson Research Center, 3615 Civic Center Blvd, Suite 502-G, Philadelphia, PA, USA. E-mail: jhwolfe@vet.upenn.edu*

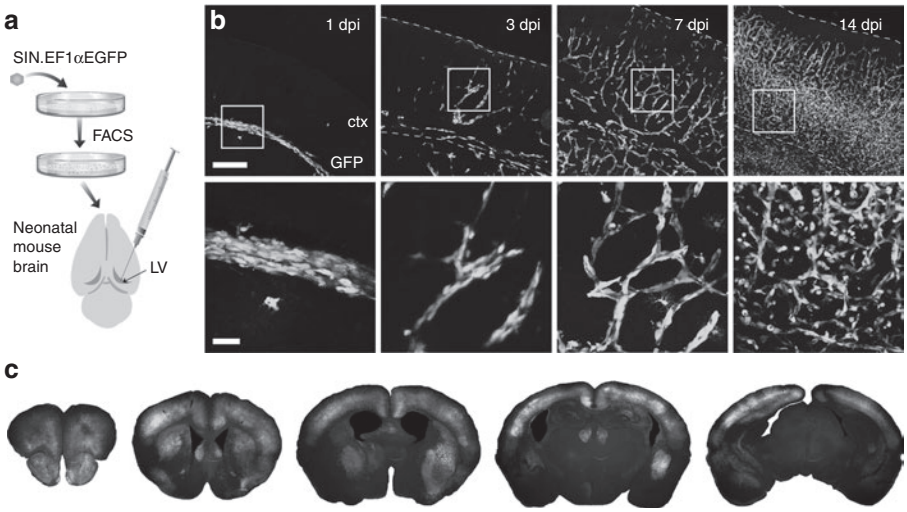

Figure 1 Engrafted neural stem cells (NSCs) migrate and proliferate extensively during first two postnatal weeks. (**a**) Schematic illustration of intraventricular NSC transplantation in neonatal rodent brain. (**b**) Trajectory of transplanted NSCs during first two postnatal weeks. Lower panels are magnified view (4x) of boxed region in upper panels. (**c**) Representative coronal sections along rostrocaudal axis features stable cortical grafts at 8 wks post-transplant. (Scale bars in **b**: 250 µm, *Upper*; 50 µm, *Lower*).

through a mechanism not requiring GABAergic neurotransmission. Furthermore, our study revealed that there was a significant dose-dependent depletion of host cells within engrafted regions. We demonstrate that nonintegrating NSCs can induce differential network alterations as a function of engraftment level, which puts a premium on methods used to derive donor cells as well as appropriate controls for engraftment effects.

RESULTS

Distribution and differentiation of grafted NSCs

To evaluate the functional impact of exogenous NSCs on host cortical networks *in vivo*, we used the immortalized NSC line C17.2 in an established murine transplantation model[22] (**Figure 1a**). C17.2 cells are amenable to expansion and genetic manipulation *in vitro*, and able to migrate and survive long-term *in vivo*[22–26] compared with primary-derived cells.[8,19] The NSCs were modified to constitutively express green fluorescent protein (GFP) and injected intraventricularly into the neonatal (P0-P2) mouse brain.[22] At 1-day postinjection, donor NSCs occupied periventricular regions (**Figure 1b**), at 3-day postinjection, we observed chains of migrating NSCs, and by 14-day postinjection, *in vivo* expansion resulted in robust cortical engraftment throughout the neuroaxis (**Figure 1c**). To phenotype donor cells, we performed immunofluorescence analysis 2 months after transplant (**Figure 2**), which showed that engrafted NSCs remained in a largely nonproliferative, undifferentiated state.

Dose-dependent effects on amplitude of cortical activation

We previously found that stable engraftment of ectopic NSCs caused no gross behavioral abnormalities.[22] However, it is unclear whether high density of engraftment in some areas could disrupt existing neural networks. To investigate whether cortical dynamics were influenced by engraftment density, NSC levels were titrated *in vivo* using three different input doses (80,000, 40,000, and 8,000 cells/ventricle). We quantified engraftment using two-dimensional confocal projections of each slice and expressed values as percent GFP-positive area normalized to total cortical area (**Figure 3a**). Automated cell counts on an independent set of slices validated this measurement method. Graft area measurements strongly correlated to cell counts (Pearson's correlation $r = 0.99$ $P < 0.0001$), and thus served as a metric for NSC engraftment level (**Figure 3b–e**).

Optical recordings were made in acute slices of somatosensory cortex at 2 months post-transplant in response to a single callosal stimulation (**Figure 4a**, **b**). We observed a progressive reduction in peak signal amplitude ($\Delta F/F_0$) with increased cortical engraftment, suggesting that exogenous NSCs can modulate network excitability (**Figure 4c**). To determine the locus of dampened cortical activity, we generated color-coded maps depicting maximum $\Delta F/F_0$ for individual pixels across all movie frames (**Figure 4d**). We observed a strong negative correlation between engraftment level and corresponding peak $\Delta F/F_0$ values (Pearson's correlation $r = -0.82$; $P < 0.0001$) (**Figure 4e**). K-means clustering of maximum $\Delta F/F_0$ values partitioned the slices into three engraftment densities: control, moderate, and high (**Figure 4f**). We expressed engraftment as percent GFP-positive area normalized to total cortical area. Whereas high levels (>25%) caused marked reductions in the amplitude of activation (0.10 ± 0.01 versus $0.22 \pm 0.01\%$, $P < 0.0001$), moderate levels (<15%) did not alter this network property (0.19 ± 0.01 versus $0.22 \pm 0.01\%$, $P > 0.05$). Furthermore, the injection procedure itself did not significantly perturb host physiology (**Supplementary Figure S1a,b**). Collectively, these data indicate that network alterations induced by exogenous NSCs are dose dependent.

Spatiotemporal patterns of cortical excitation

We next investigated the spatiotemporal patterns of excitation across engraftment densities (**Figure 5a**,**b**). Consistent with earlier work,[15,27] a single stimulus-activated deep layers (L5/6) in control slices (see frames at 3 and 6 ms), followed by columnar activation to L1 with simultaneous horizontal spread in L5/6 (see frames at

8 and 10 ms). Within superficial layers (L2/3), excitation propagated laterally (see frames at 14 and 18 ms). Moderately engrafted slices showed activity patterns similar to control, whereas highly engrafted slices exhibited columnar activity with minimal lateral spread. To quantify the global extent of activation, we determined the number of pixels that exhibited significant depolarization after callosal stimulation. The activated pixel number in a defined cortical region was normalized against the total pixel number, generating an activation measure, and plotted against time. Time of peak activation, rise time, and fall time extrapolated from these plots were not significantly altered across engraftment densities, suggesting that aspects of cortical function were preserved in this transplantation model. However, the maximum activated area negatively correlated to engraftment level (Pearson's correlation $r = -0.78$, $P < 0.0001$) (**Figure 5c**). Furthermore, whereas high levels of ectopic cells spatially constrained activity (0.81 ± 0.12 versus $1.94 \pm 0.12\,mm^2$, $P < 0.0001$), moderate levels maintained excitatory spread across lamina (1.52 ± 0.10 versus 1.94 ± 0.12, $P > 0.05$) (**Figure 5d**). These results suggest that undifferentiated NSCs, at high levels, block the horizontal propagation of excitatory potentials, while preserving columnar connectivity in the somatosensory cortex.

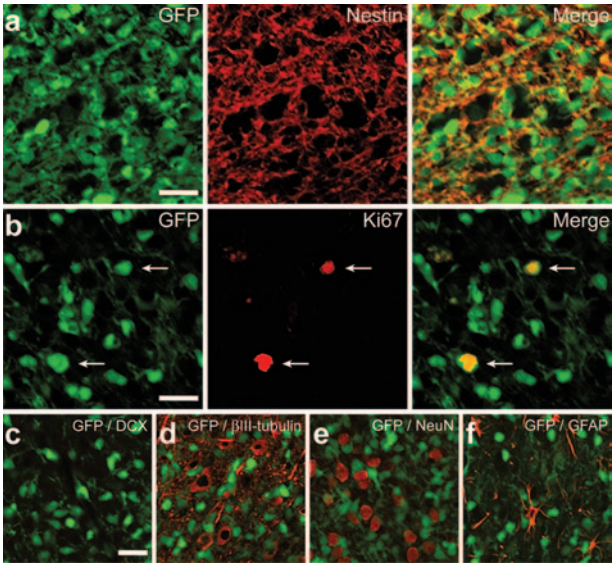

Figure 2 Exogenous neural stem cells (NSCs) show limited differentiation potential *in vivo*. (**a**) Cortical grafts are immunopositive for nestin, a marker of undifferentiated NSCs, at 8 weeks post-transplant. (**b**) GFP-labeled cells were largely quiescent, with only a small percentage continuing to proliferate, as indicated by Ki67 immunonoreactivity. (**c**-**f**) Exogenous NSCs show no evidence of differentiation into mature neural lineages, as suggested by absence of DCX, βIII-tubulin, NeuN, and GFAP colabeling. (Scale bars: 25 μm).

Defects within laminar circuits

Spatiotemporal properties of cortical activity are determined by interactions between local laminar and columnar circuits.[13,28] Therefore, we examined the effect of exogenous NSCs on cortical layers (L2-L6), approximated by horizontally aligned bins that were perpendicular to the axis of columnar activity (**Figure 6a**). Bin 1 and 2 corresponded to the supragranular layers (L2/3), bin 3 aligned with layer 4; and bins 4 and 5 largely represented infragranular layers (L5/6). In each binned response (**Figure 6b**),

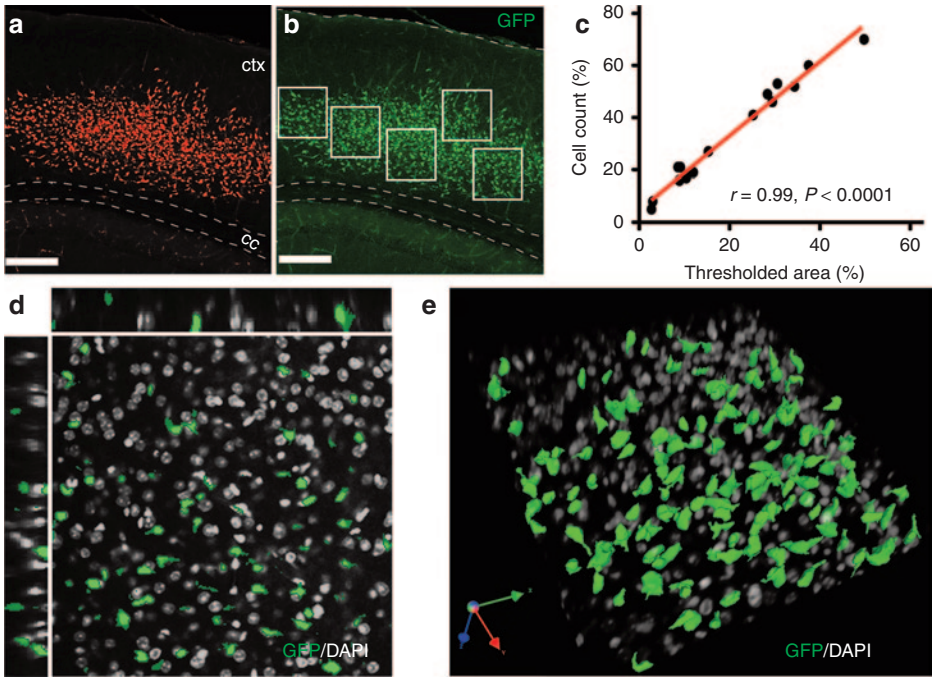

Figure 3 Exogenous neural stem cells exhibit robust levels of engraftment in cortex. (**a**) Maximum intensity projection showing thresholded GFP+ graft at 8 weeks (red mask represents all pixel intensities ≥2 SD above mean background intensity). (**b**) Automated counts performed on five randomly selected cortical regions of interest (ROIs) (white boxes) validate graft area measurements. (**c**) Correlation plot with linear fit comparing quantitation methods from **a** and **b** ($n = 16$ slices). (**d**) Representative optical plane from engrafted ROI in **b** showing colocalization of GFP and DAPI fluorescence. (**e**) 3-D reconstruction of engrafted ROI in **b** rendered from confocal z-stack. (Scale bars in **a** and **b**: 250 μm).

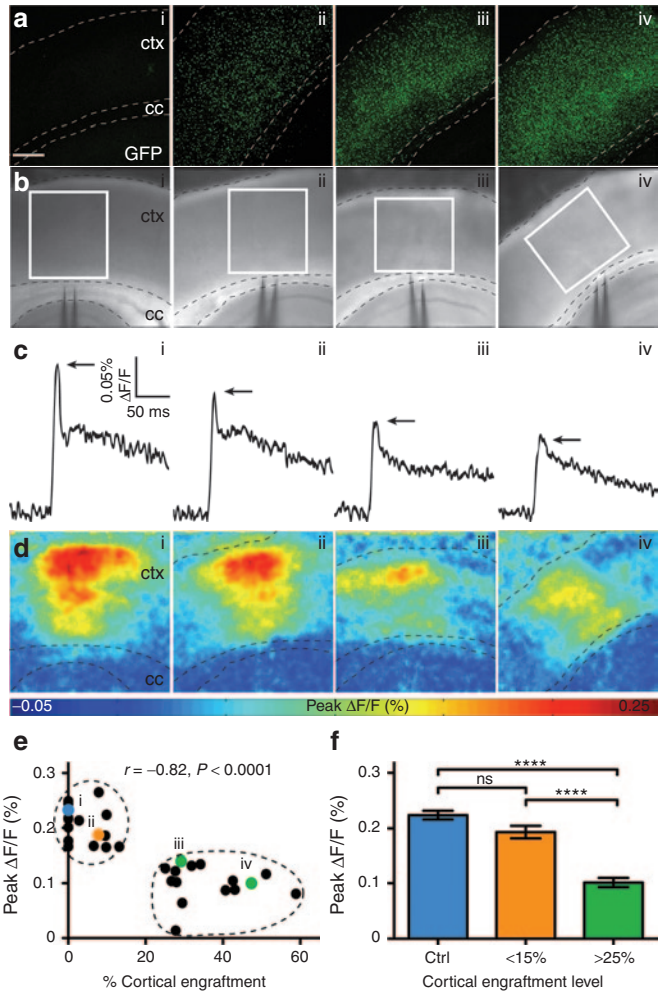

Figure 4 Neural stem cell engraftment reduces amplitude of cortical activation in a dose-dependent manner. (**a**) Confocal images of representative cortical grafts (i–iv) at 8 weeks. (**b**) Bright-field images showing cortical slice preparation and electrode placement for voltage sensitive dye (VSD) imaging. (**c**) VSD traces of time resolved mean fluorescence intensity change ($\Delta F/F_0$) within defined cortical region of interest (white boxes in **b**). (**d**) Color-coded maps of cortical activation, depicting maximum F/F_0 for individual pixels within a 1024 ms recording interval. (**e**) Correlation plot of maximum signal amplitude versus cortical engraftment level (n = 33 slices). (**f**) Histogram showing differential effects of engraftment on evoked VSD signal (control, n = 9; <15%, n = 9; >25%, n = 15). All imaged slices grouped into engraftment densities based on K-means clustering of maximum $\Delta F/F_0$ values (dotted circles in **e**). Data are means ± SEM (****P < 0.0001). (Scale bar in **a**: 250 µm).

we examined several indices of circuit function: peak amplitude, peak active area, peak displacement, and peak velocity of propagating potentials. Consistent with the global measures (**Figure 4e,f**), binned responses demonstrated a progressive reduction in peak $\Delta F/F_0$ (**Figure 6c**), peak active area (**Figure 6d**), and peak horizontal displacement (**Figure 6e**) with increased engraftment density. The peak propagation velocity was calculated as the maximal difference in active area between any two consecutive movie frames over the imaging interval. While layer-specific velocity was reduced in all bins of highly engrafted slices, moderately engrafted slices showed pronounced defects in deep layers exclusively (0.70 ± 0.04 versus 0.99 ± 0.06 mm/ms, P < 0.05) (**Figure 6f**).

The temporal and spatial integration of afferent inputs is critical to the formation of complex representations during wake states.[29] Repetitive callosal stimuli were applied at two frequencies, 10 and 40 Hz, to mimic prevailing rhythms present *in vivo* during slow wave sleep and activated states, respectively. Both stimulation trains are known to produce facilitating responses in the rodent somatosensory cortex.[15] High levels of exogenous NSCs blocked the enhancement of peak $\Delta F/F_0$ in all cortical bins (**Figure 6g,h**). Facilitation was differentially impaired in bin 4 (1.63 ± 09 versus 2.08 ± 0.13 mm^2, P < 0.05) and bin 5 (1.46 ± 0.07 versus 1.95 ± 0.13, P < 0.01) of moderately engrafted slices. These data indicate that moderate NSC levels cause measureable defects in cortical computations within infragranular circuits.

Early implantation exposes NSCs to endogenous growth signals that promote rapid graft expansion, causing both mild and severe defects to host physiology. To determine whether such deficits are induced following delivery into the mature brain, NSCs were stereotaxically injected into the left cortical hemisphere of adult mice. Vehicle (mock) injections were administered to the right hemisphere to control for effects induced by the injection route. Mock injected responses were indistinguishable from those in uninjected controls. Grafts established 2 months post-transplant did not exceed moderate levels. Consistent with neonatal transplants, this level of engraftment did not perturb gross measures of host function (amplitude, area, displacement, and velocity) (**Supplementary Figure S2a–d**). Interestingly, a more subtle measure of network function (integration of repetitive inputs in deep layers), that was disrupted in neonatal transplant recipients, was not altered in adult recipients (**Supplementary Figure S2f**). These results suggest that the developmental stage of the host brain can largely influence functional outcome of cell therapies; however, engraftment in adult transplants is limited to the area of injection.

Alterations to excitatory and inhibitory network tone

NSC-induced alterations in cortical excitability may be a consequence of either reduced excitatory or enhanced inhibitory network tone.[15,30,31] To distinguish between these two possibilities, we blocked γ-Aminobutyric acid type A receptor ($GABA_AR$)-mediated inhibition with picrotoxin (PTX). Cortical responses to single callosal stimuli were monitored before and 30 minutes after PTX treatment. Control and highly engrafted slices exhibited PTX-induced hyperexcitability, as shown in color-coded activity maps (**Figure 7a**). Suppression of GABAergic signaling expanded the boundaries of cortical activation (**Figure 7a**) and also, prolonged depolarizing responses in all cortical bins (**Figure 7b**). Differences in the magnitude of excitation pre- and post-PTX application were comparable in all cortical bins of control and highly engrafted groups, except in bin 4 (0.010 ± 0.001 versus 0.007 ± 0.001, P < 0.05) (**Figure 7c**). We conclude that host neurons can be recruited, even in the presence of many exogenous NSCs, to increase cortical excitation. However, our results also suggest that ectopic cells differentially impaired infragranular excitatory circuits. Grafted NSCs markedly lowered the absolute level of excitation attained following PTX treatment in bin 3 (0.80 ± 0.10 versus 1.20 ± 0.07%, P = 0.02), bin 4 (0.76 ± 0.10 versus 1.20 ± 0.07%, P = 0.006), and bin 5 (0.71 ± 0.09 versus 1.00 ± 0.07%, P = 0.02) (**Figure 7d**). These

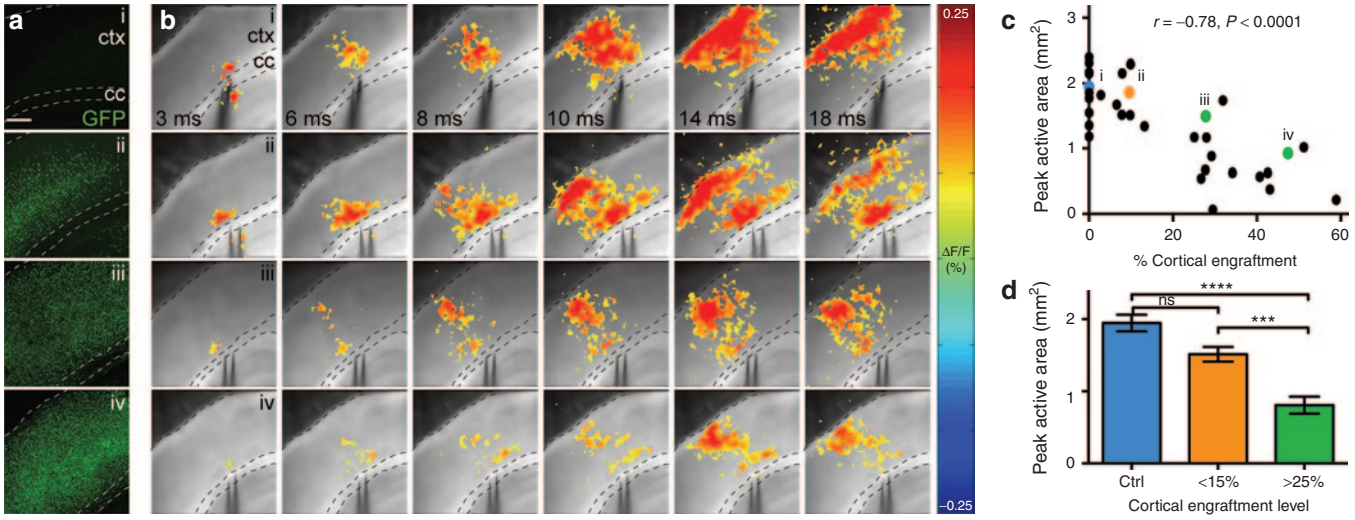

Figure 5 Stereotypic pattern of cortical excitation is conserved but spatially restricted at high engraftment levels. (**a**) Confocal images of representative cortical grafts (i–iv) at 8 weeks. (**b**) Spatiotemporal maps of cortical activity following callosal stimulation. For each representative slice, corresponding series of frames shows pattern of voltage sensitive dye signal propagation. (**c**) Correlation plot of maximum activated area versus cortical engraftment level (n = 33 slices). (**d**) Peak area of cortical activation is smaller in highly engrafted (green bars) but not significantly altered moderately engrafted slices (red bars), (control, n = 9; <15%, n = 9; >25%, n = 15). Data are means ± SEM (***P < 0.001, ****P < 0.0001). (Scale bars in **a**: 250 µm).

data indicate that grafted NSCs reduced the excitatory network tone in deep layers. Furthermore, we can conclude that exogenous cells do not require $GABA_AR$ signaling mechanisms to modulate network activity. GABA-A signaling may partially contribute to observed alterations; however, this is coupled with additional changes to either excitatory connections or the intrinsic excitability of host neurons.

Depletion of host cells in engrafted cortices

We observed a depletion of DAPI+/GFP- host cells in the cortex, which strongly correlated with engraftment level (Pearson's correlation r = 0.99, P < 0.0001) (**Figure 7e**). No concomitant change to cortical thickness was detected. We also performed a microcircuit analysis of lightly and heavily engrafted regions within the same acute slice preparation. Based on this analysis, we found that host cell number is negatively correlated to donor cell number (Pearson's correlation r = −0.60, P < 0.0001, n = 78 regions) (**Figure 7f**). In all cases, total cell number was conserved across control, moderate, and high-density engraftment conditions (P = 0.14) as indicated by automated DAPI counts averaged across five regions of interest (**Figure 7g**). We also observed marked neuronal depletion in subcortical regions, based on NeuN quantification within engrafted striatal tissue (11.27 ± 2.42 versus 26.92 ± 1.10, P < 0.0001) (**Supplementary Figure S1c**). In engrafted striatal regions, the number of neurons also varied inversely with total number of cells (Pearson's correlation r = −0.62, P < 0.05, n = 15 regions) (**Supplementary Figure S1d**). Collectively, these results indicate that engraftment of NSCs was gained at the cost of endogenous cells.

DISCUSSION

Transplanted NSCs have the potential to provide therapeutic benefit in a number of disease states through gene or drug delivery, cell replacement, or by exerting trophic or neuroprotective effects. However, there has been considerable difficulty achieving efficient integration of implanted cells, independent of source.[3–7] In the current study, we used a NSC line that remains undifferentiated in the cortex to investigate the physiological effect of nonintegrating NSCs across a range of engraftment levels. Based on VSD imaging of network dynamics, we found that the cortex can safely accommodate quantities of immature cells comparable with those currently attained from primary NSCs, ES-NSCs, and iPS-NSCs. At levels of engraftment up to 15%, we observed subtle yet, physiologically relevant disruptions to network function exclusively in deep cortical layers (L5/6). However, at very high levels of engraftment (exceeding 25% engraftment), there were much more extensive and severe alterations to activity, specifically to the amplitude, spatial extent, and velocity of propagating potentials. The results suggest that a threshold of inefficiency in integration may confound analysis of deficits in models of neurological disease and interfere with the therapeutic effect of cell therapy.

These data are consistent with the findings that ectopic C17.2 cells can functionally interact with host circuits well before electrophysiological maturation.[32] In this previous study, grafted NSCs were engineered to overexpress neurotrophin-3, which allowed them to differentiate into neurons and form gap junctions with host neurons. Gap junctions lower the input resistance of coupled cells in the developing cortex,[33] and provide a mechanism by which grafted cells could lower the intrinsic excitability of intact host neurons. However, we found no evidence of gap junction formation between grafted, unengineered NSCs, and endogenous cells (data not shown). Therefore, the cellular mechanism underlying circuit interference remains unclear.

One possibility is that exogenous cells used GABA-dependent mechanisms to modulate cortical excitability. GABAergic inhibition plays a pivotal role in shaping the spatiotemporal properties of evoked cortical responses *in vitro*[15,30] and *in vivo*,[31] including the integration of afferent inputs.[34] Transplanted primary

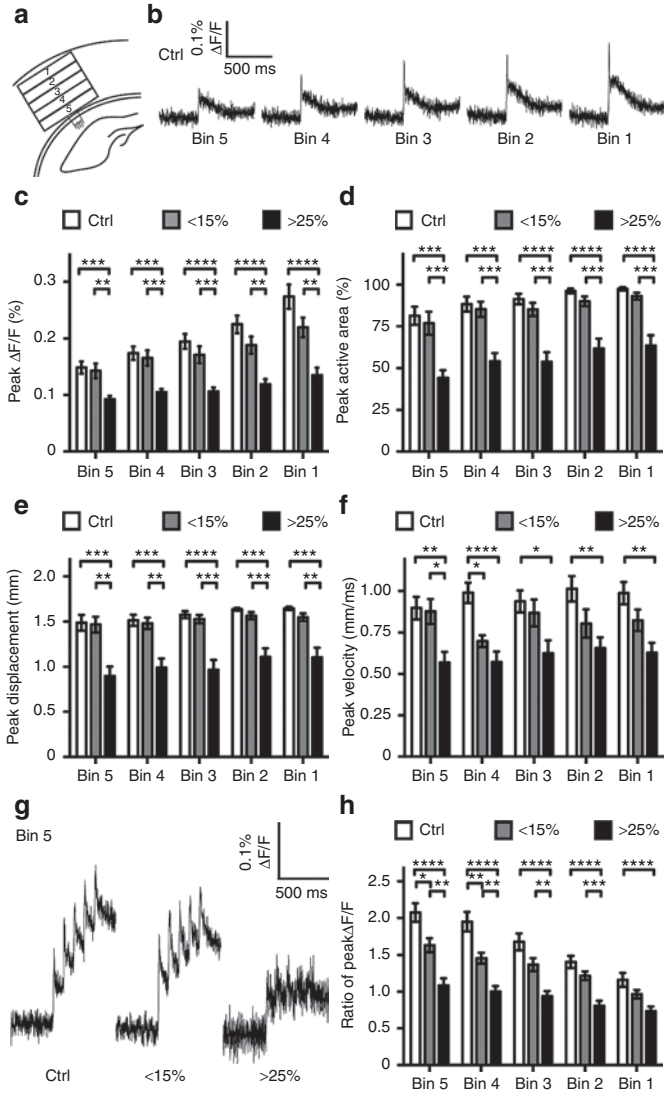

Figure 6 High levels of cortical engraftment lead to layer-specific disruptions in network function. (**a**) Schematic illustration of spatial binning within a neocortical region of interest (ROI). For each imaged slice, five horizontally aligned bins were generated, each perpendicular to the axis of columnar activity. (**b**) Representative traces showing evoked voltage sensitive dye (VSD) response within cortical bins of a control slice. (**c**-**f**) Histograms demonstrating effect of engraftment on VSD signal properties in binned cortical regions (control, $n = 9$; <15%, $n = 9$; >25%, $n = 15$). Peak intensity (**c**), activated area (**d**), displacement (**e**), and propagation velocity (**f**) of potentials are significantly altered across cortical bins of highly engrafted slices (green), but not in moderately engrafted slices (red bars). (**g**) Representative traces showing evoked VSD response in bin 5 to repetitive stimuli (5 pulses, 10 Hz) across engraftment conditions. (**h**) Comparison of facilitating responses across cortical bins and engraftment conditions (control, $n = 9$; <15%, $n = 9$; >25%, $n = 15$). Shown are ratios of peak $\Delta F/F_0$ signal (fifth response is normalized to first response) after repetitive callosal stimulation. Data are means ± SEM (*$P < 0.05$, **$P < 0.01$, ***$P < 0.001$, ****$P < 0.0001$).

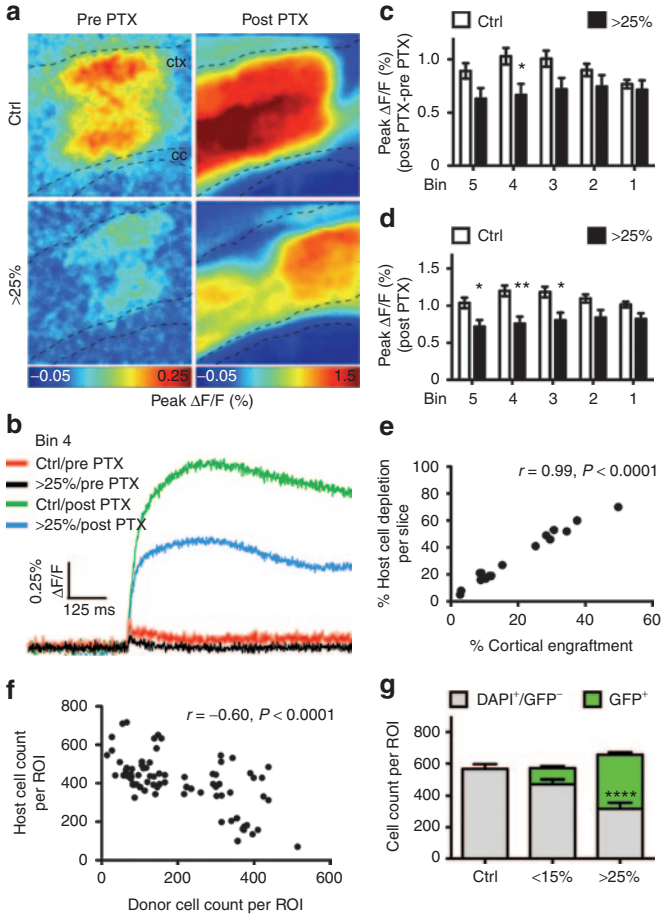

Figure 7 Ectopic neural stem cells impair excitatory network structure in deep layers and induce host cell depletion. (**a**) Color maps of cortical activation, depicting maximum $\Delta F/F_0$ for individual pixels within a 1024-ms interval. Representative maps show effect of $GABA_A$ receptor antagonist, PTX, on cortical activity in control (Upper) and highly engrafted (Lower) slices. Note that both control and engrafted slices exhibit PTX-induced hyperexcitability (left panels, baseline; right panels, 30 minutes after picrotoxin application). (**b**) Representative optical recordings from control and highly engrafted slices pre- and post-PTX treatment. (**c**) Histogram showing relative change in excitability (post-PTX – pre-PTX) following drug application ($n = 5$). (**d**) Histogram displaying peak $\Delta F/F_0$ values during blockade of GABAergic inhibition ($n = 5$). (**e**) Correlation plot showing depletion of DAPI+/GFP host cells versus cortical engraftment level across imaged slices ($n = 16$) at 8 weeks. (**f**) Correlation plot showing host (DAPI+/GFP-) versus donor (DAPI+/GFP+) cell count across imaged ROIs ($n = 78$) at 8 weeks. (**g**) Histogram showing endogenous (gray bar) and donor (green bar) cell count by ROI across engraftment conditions (control, $n = 9$; <15%, $n = 9$; >25%, $n = 7$). Total cell count is preserved across conditions ($P = 0.14$) highly slices ($n = 7$) at 8 weeks. Data are means ± SEM (*$P < 0.05$, **$P < 0.01$, ***$P < 0.001$, ****$P < 0.0001$).

embryonic cerebellar and cortical tissue, rich in GABA, can raise thresholds for seizure initiation in rodent models of epilepsy.[35] Furthermore, transplanted neural precursors isolated from the medial ganglionic eminence (MGE) can differentiate into mature cortical interneurons that increase local inhibition[10] or globally suppress seizure activity in the epileptic brain.[36] These findings suggest that transplantation of GABAergic progenitor cells is sufficient to markedly dampen host activity. However, donor cells in our study were not GABAergic, as indicated by negative GAD67 immunolabeling (data not shown). We also performed $GABA_AR$ blockade experiments to test whether ectopic NSCs potentiated inhibitory neurotransmission in the host cortex. Application of the GABAergic antagonist picrotoxin to acute slices revealed all latent excitatory connections. Preservation of activity in the presence of drug would suggest that excitatory network structure is intact within engrafted cortices and that functional alterations are

mediated exclusively by enhanced GABAergic signaling. However, we found that activity within deep cortical layers was significantly reduced in picrotoxin-treated engrafted slices, suggesting that that donor cells potentially disrupted the number, trajectory, or targeting of excitatory host cells or their pathways.

NSC-induced activation of cellular intermediates, such as resident astrocytes and microglia, may also alter host neuronal activity. However, these cell types have been shown to increase neural excitability, and are therefore, unlikely to dampen circuit activity in our model. Astrocytic gliosis has been found to generate deficits in neuronal inhibition by inducing GABA depletion.[37] Astrocytosis-mediated deficits in inhibition further trigger hyperexcitability in hippocampal circuitry. Microglial activation can also induce astrocyte-mediated potentiation of excitatory neurotransmission.[38] Activated microglia act on astrocytes through purinergic signaling, which triggers glutamate release. Activation of downstream neuronal metabotropic glutamate receptor 5 enhances frequencies of excitatory postsynaptic currents (EPSCs). However, elevated EPSC frequencies are not consistent with our reported reduction in cortical excitability. It has also been reported that resident microglia provide trophic support to endogenous neurons in deep cortical layers postnatally,[39] and thus, are unlikely to account for neuronal depletion in our system. Inflammatory mediators have been shown to decrease current thresholds of action potential generation in both intact and dissociated neurons, leading to a hyperexcitable phenotype.[40] However, we found that engrafted slices had elevated, not reduced, thresholds of cortical activation, as determined by local field recordings (**Supplementary Figure S3**).

We did observe a dose-dependent depletion of host cells in engrafted regions, with no concomitant changes in cortical thickness. The total cell number was conserved, suggesting that endogenous cells were lost. Consistent with this finding, neuron numbers in subcortical regions were reduced with increased numbers of exogenous cells. Competition for external trophic signals in the host brain may mediate this loss. Trophic requirements have been shown to tightly regulate total cell number in the cerebral cortex. The size of interneuronal grafts in the normal rodent brain has been restricted in this way, with a number of precursors undergoing apoptosis to maintain a fixed cell number.[41] Furthermore, programmed cell death has been found to restrain cell number in the developing cortex.[42] Therefore, it is possible that grafted NSCs compete with resident excitatory neurons for trophic support, leading to increased death of endogenous cells.

The loss of host cells is sufficient to substantially diminish cortical network excitability, as evidenced by previous studies.[43] We found the physiological effects of host cell depletion to be more nuanced in our model. Whereas moderate engraftment depleted endogenous populations to levels that affected network integration, high engraftment was required to deplete host cells to levels that globally impaired activity. Our results also suggest that grafted NSCs preferentially affect infragranular circuits. Although moderate engraftment largely preserved cortical function, these levels noticeably reduced the velocity of signal propagation and blockedfacilitation in L5/6. Moreover, excitatory infragranular circuits, unmasked by PTX application, showed dampened activity in highly engrafted slices. These results are consistent with the cortical distribution of grafted NSCs, which localized to deep cortical layers. We did, however, observe alterations to the peak amplitude, spatial extent, and velocity of potentials in L2/3, suggesting that supragranular circuit function is also disrupted to some degree.

We propose that functional defects in L2/3 of highly engrafted slices may be the result of columnar interactions with underlying L5/6. Recent findings have shown that blocking L5 activity with tetrodotoxin (TTX) significantly reduces peak $\Delta F/F_0$ signal throughout the depth of the cortex, suggesting that L5 amplifies activity in L2/3.[27] Therefore, high levels of exogenous NSCs in L5/6 may contribute to the reduction of $\Delta F/F_0$ signal in L2/3 that we observed. Additionally, high levels of engraftment blocked the lateral spread of excitation in L2/3. Local inactivation of L5 with TTX produces a similar effect,[27] suggesting that defects in L2/3 signal propagation may be attributed to reduced L5 input. Layers 2/3 have sparse connectivity, with 10 times as many inhibitory connections as excitatory connections,[44] and more hyperpolarized neurons.[28,45] Therefore, L2/3 requires powerful excitatory drive from L5 to depolarize. Accordingly, when inhibitory input was pharmacologically suppressed with PTX in our study, superficial layers sustained activity without L5 input. Additionally, L2/3 blockade with TTX does not significantly alter $\Delta F/F_0$ in the cortex and only minimally affects activation of surrounding columns.[27] These results indicate that impairment to L5 function alone is sufficient to influence activity in superficial cortical layers. We propose that exogenous NSCs may directly interfere with infragranular circuitry by altering the number of host cells, and consequently, the number of functional synapses. Sparse L5/6 connectivity may reduce excitatory input to L2/3, interfering with the initiation and lateral propagation of activity within L2/3, which is consistent with our results.

Overall, our study has a number of implications for cell therapy in the central nervous system. In particular, these data put a premium on the method used to obtain cells as well as appropriate controls for engraftment. A number of studies have demonstrated that fully differentiated grafts can preserve host function, suggesting that alterations in our study are due to nonintegrating cell types. For example, the cortex can accommodate a large number of ectopic, fully differentiated interneurons without significant alteration to activity.[41] Transplantation of interneuronal progenitors expanded the cortical interneuronal population by up to 35%, but the frequency of inhibitory synaptic events did not scale up proportionately. Moreover, it has been shown that transplanted ES-derived neurons can adopt and drive activity of endogenous hippocampal networks.[46,47] Finally, mature NT2N neurons derived from a clonal human teratocarcinoma line (NT2) have been transplanted in phase I[48] and II[49] clinical trials for stroke therapy. These cells, selected for their potent neuronal lineage commitment, did not cause deleterious effects in affected patients. Collectively, these studies suggest that the host brain can safely accommodate fully differentiated cells.

Additionally, our findings establish a limit for the number of engrafted progenitors in cortex. Low levels of engraftment have been achieved with primary NSCs[8,19] and other NSC lines,[20,21] but such levels are likely to be subtherapeutic.[50] Similarly, adult parenchymal transplants resulted in limited cortical engraftment.

Although these levels were well tolerated by the adult recipients, they restrict the utility of NSCs for the treatment of widespread pathology of neurogenetic diseases. Optimization of graft survival and migration using genetic engineering may improve therapeutic outcomes through enhanced distribution of the NSCs. However, our data also suggest that such improved engraftment levels may also introduce defects in the network function, which may interfere with the beneficial effect of the cell therapy. It will be necessary to find a balance between the engrafted cell density that is needed for a therapeutic effect and preserving normal host circuit functions.

MATERIALS AND METHODS

Cell culture, labeling, and sorting. The C17.2 line was derived after v-myc immortalization of progenitor cells isolated from the postnatal mouse cerebellum.[17] NSCs were maintained as an adherent monolayer on uncoated 10-cm dishes at 37°C and 5% CO_2 and passaged at a ratio of 1:10 by trypsinization twice per week. Growth medium contained 83% Dulbecco's modified Eagle's medium with glucose (4.5 g/l) and 1 mmol/l sodium pyruvate, 10% fetal bovine serum, 5% horse serum, 1% L-glutamine, and 1% penicillin-streptomycin-fungizone (all from Gibco, Grand Island, NY). Lentiviral-mediated labeling of C17.2 cells was performed as described previously to enable reliable graft identification.[18] A self-inactivating (SIN) lentiviral vector driving constitutive EGFP expression from the human elongation factor 1α promoter (EF1α) was generated using standard triple transfection approach.[18] C17.2 cells were transduced for 12 hours in conditioned medium containing the vector (SIN.EF1 α.EGFP) at multiplicities of infection of approximately 10. Labeled populations were sorted for EGFP on the FACSVantage SE cell sorter (BD Biosciences, San Jose, CA) and expanded *in vitro* following recovery for two additional passages prior to transplantation. EGFP has been used as a reporter gene in a number of other transplantation studies without observable alteration to donor cell physiology.[7,9,10] Additionally, several genetic voltage and calcium indicators, developed to reliably monitor cell physiology, are EGFP fusions.[51,52] EGFP toxicity has not been observed using these functional reporters. Therefore, it is unlikely that functional outcomes in this study are the result of some unknown impact of EGFP expression.

Neonatal transplantation. Cells were harvested for transplantation as previously described.[18] Briefly, cells were trypsinized and washed twice in PBS before final resuspension in PBS to yield a final concentration of 40,000 cells/μl. Only viable cells, determined using trypan blue exclusion, were included in cell counts. For the dose-response study, cell preparations were serially diluted in PBS. Mice were divided into four groups according to the number of input cells/ventricle: 80,000 ($n = 3$), 40,000 ($n = 3$), 8,000 ($n = 3$), and uninjected ($n = 3$). During the transplantation procedure, the heads of cryoanesthetized neonatal (P0-2) C57BL/6 mice were transilluminated and approximately 2 μl of cell suspension was slowly injected into each lateral ventricle with a finely drawn glass micropipette. The angle of injection is such that the needle does not penetrate through the somatosensory cortex, but instead enters through caudal aspect of the brain to minimize tissue damage. Injected pups were warmed up and returned to maternal care after recovery. All procedures were approved by the Institutional Care and Use Committee at the Children's Hospital of Philadelphia.

Stereotaxic adult injections. All animals receiving injections were older than 2 months of age at the time of injection. Under sterile conditions, SCID mice ($n = 4$) were anesthetized with isofluorane and secured in a stereotaxic frame (David Kopf Instruments, Tujunga, CA) and holes the size of the injection needle were drilled into the skull. Cell injections were done unilaterally with 0.5 μl of suspension (40,000 cells total). An equivalent volume of PBS was injected into the contralateral hemisphere. The injection syringe (Hamilton, Reno, NV) delivered cells or vehicle at a constant volume of 0.1 μl/minutes using a syringe pump (KD Scientific, Holliston, MA). The needle was left in place for 3 minutes after each injection to minimize upward flow of viral solution after raising the needle. Coordinates [in millimeters; rostral (+) or caudal (−) to bregma, left of midline, ventral to pial surface] for the cortex were −2.1, 1.25, and 1.1. All procedures were approved by the Institutional Care and Use Committee at the Children's Hospital of Philadelphia.

Cortical slice preparation. Brains were harvested from both neonatal and adult recipients 8–10 weeks post-transplant for live imaging. Mice were anesthetized with isoflurane, decapitated, and the brains removed and blocked in ice-cold artificial cerebral spinal fluid (ACSF) (3 mmol/l KCl, 1.25 mmol/l $NaHPO_4$, 1 mmol/l $MgCl_2$, 2 mmol/l $CaCl_2$, 26 mmol/l $NaHCO_3$, 10 mmol/l glucose), in which NaCl was replaced with an equal osmolar concentration of sucrose (130 mmol/l). After removal of the cerebellum, the two hemispheres were separated with a midsagittal cut, and each hemisphere was mounted for sectioning. Coronal slices (350 μm) at the level of the hippocampus were cut with a vibratome (VT1200S, Leica, Buffalo Grove, IL) and transferred into ACSF without sucrose. Slices were subsequently placed on tea paper, transferred to a holding chamber (37°C) for a 45 minute-recovery period, and then stored at room temperature for up to 6 hours.

Confocal imaging and analysis. Following recovery, acute cortical slices were transferred to an ACSF-filled imaging chamber for confocal microscopy. GFP-positive grafts were imaged at x10 magnification using a confocal-scanning laser microscope (FluoView1000, Olympus, Center Valley, PA). Stacks of consecutive brightfield and confocal images were taken simultaneously at 10 μm intervals and acquired using an argon laser (488 nm). All analyses were performed using ImageJ software (NIH, Bethesda, MD). A maximum intensity projection was generated from each Z stack and a region of interest (ROI) was drawn around the entire neocortex using the corpus callosum as the ventral border. The percentage of pixels with intensities more than two standard deviations above the background pixel intensity was quantified for each slice. Graft measurements were validated with automated cell counts performed on five randomly-chosen ROIs in control ($n = 9$) and engrafted slices ($n = 16$) using Volocity software (PerkinElmer, Waltham, MA). The number of GFP-positive cells per ROI was quantified and normalized to the total number of DAPI positive. In subcortical regions, including the striatum, NeuN- and DAPI-positive cells were quantified per ROI using automated methods available through Fiji software.[53]

Immunohistochemistry. Engrafted cells were phenotyped using standard immunohistochemistry. At 8 weeks post-transplant, brains were removed and fixed in 4% paraformaldehyde/PBS after transcardial perfusion. Harvested brains were embedded in 2% agarose and sectioned coronally at 50 μm on a vibratome (Leica VT1000S, Leica, Buffalo Grove, IL). Free-floating sections were postfixed in 4% PFA in PBS for 20 minutes, then permeabilized and immunoblocked at room temperature for 1 hour in PBS containing 2.5% goat or donkey serum and 0.2% Triton X-100. Slices were then incubated overnight at 4°C with primary antibodies against the following antigens: GFP (1:1,000, Molecular Probes, Grand Island, NY), Nestin (1:500, Millipore, Billerica, MA), Ki67 (1:200, Novoscastra, Buffalo Grove, IL), DCX (1:200, Santa Cruz, Dallas, TX), βIII-Tubulin (1:1,000, Millipore, Billerica, MA), NeuN (1:500, Millipore, Billerica, MA), and GFAP (1:1,000, Millipore, Billerica, MA). After three washes in PBS, sections were incubated at room temperature for 2 hours with appropriate secondary antibodies conjugated to Alexa 594 or 488 (Molecular Probes, 1:300, Grand Island, NY). All antibodies were diluted in PBS. After several washes, slices were mounted in Vectashield with DAPI (Vector Labs, Burlingame, CA) and examined with a confocal scanning-laser microscope. Confocal images from a single optical plane were acquired sequentially with two lasers (argon, 488 nm; helium/neon, 543 nm) at x20 magnification with optical zoom of 2 or 5. Image processing was carried out using ImageJ software.

Local field recordings and analysis. Acute cortical slices from uninjected controls ($n = 7$) and animals injected with 80,000 cells per ventricle ($n = 8$) were assayed. Field electrodes were placed at one of the three positions

along neocortical layer 2/3. All recordings were acquired under current clamp conditions in response to a single callosal stimulation delivered via bipolar electrodes. Threshold current amplitude (x) was determined empirically. Recordings were obtained in response to current steps of x, 2x, 4x, 6x, and 8x. Five trials were obtained at each step with a 10-second intertrial interval. All analyses were performed with Clampfit software (Molecular Devices, Sunnyvale, CA).

Optical recordings. Optical responses to callosal stimuli were characterized in cortical slices ($n = 33$) across four dose conditions in neonatal recipients. Slices ($n = 8$) from injected animals without established grafts were also included in the study. Slices were dyed with di-3-ANEPPDHQ (Molecular Probes) in ACSF for 15 minutes, placed in an oxygenated interface chamber, and imaged using a fast CCD camera (NeuroCCD, RedShirtImaging, Decatur, GA) with 80×80 pixel matrix and 1 kHz frame rate. Epi-illumination was provided by a Xenon lamp driven by a stable power supply. With the 4x objective, the imaging field covered the area of 1.92×1.92 mm including neocortex and underlying corpus callosum. Electrical stimulation (200 μA) was delivered by means of bipolar electrodes (World Precision Instruments, Sarasota, FL) placed on the corpus callosum. Three independent stimulation paradigms were applied (1 stimulus, 5 stimuli at 10 Hz, 5 stimuli at 40 Hz). Twelve trials were obtained per stimulation with 20 seconds elapsing between trials. Procedures were repeated for slices ($n = 18$) obtained from adult injected brains. In an independent set of experiments, we obtained recordings 30 minutes after blockade of GABAergic signaling with picrotoxin (100 mmol/l, Sigma, St. Louis, MO) in uninjected ($n = 5$) and high engrafted ($n = 5$) slices from neonatally injected brains.

VSD data analysis. Analysis of all optical data sets was performed with IGOR (Wavemetrics, Lake Oswego, OR) and software written on Matlab (Mathworks, Natick, MA). Each data set represented the average of 12 trials of stimulation. Fluorescence values for each pixel in a frame were differential, represented as the difference (ΔF) between stimulation-evoked signal and basal signal in a reference frame. A reference frame was calculated as the average of 40 frames preceding the stimulation. Intensity measurements are reported as fractional fluorescence (ΔF/F), or change in fluorescence divided by basal or resting fluorescence. Signal from an area unaffected by the stimulus was subtracted from fractional fluorescence and median filtering was applied to further reduce noise. For global assessment of cortical responses, normalized fractional fluorescence was averaged across pixels within large ROIs. Pixels with intensities above 0.1% ΔF/F (≥4 SDs over noise levels) were defined as active. Neocortical ROIs were drawn manually using white matter as the ventral border and layer I as the dorsal border. Medial and lateral borders were drawn approximately 20 pixels from a defined vertical axis of columnar activation. Regional analyses of cortical responses were performed using semiautomated software. For each slice, a vertical axis of columnar activation was defined. Five bins with fixed dimensions were generated that were oriented perpendicularly to this vertical axis. In synaptic blockade experiments, responses collected at 5-minute intervals after treatment were normalized to a baseline response obtained prior to drug application. These values were further normalized to response from ACSF (vehicle only)-treated groups.

Statistical analysis. Unpaired two-tailed Student's *t*-test and One-Way ANOVA followed by Bonferonni *post hoc* tests were used, where applicable, to determine whether mean differences between groups were different and were considered significant when $P < 0.05$. Data are reported as means ± SEM.

SUPPLEMENTARY MATERIAL

Figure S1. Functional outcomes are not directly influenced by injection route or region of engraftment.

Figure S2. Adult transplants yield levels of engraftment that do not alter host circuit function.

Figure S3. High loads of ectopic cells elevate the current threshold required to activate cortical microcircuitry.

ACKNOWLEDGMENTS

We thank Trena Clarke (Children's Hospital of Philadelphia) and Ara Polesky (University of Pennsylvania) for excellent technical assistance, and Sushma Chaubey (Children's Hospital of Philadelphia) for GFP viral vector preparation. The experiments were supported by a grant from the NIH-NINDS (R01-NS056243) to JHW; and core support from the CHOP IDDRC (P30-HD026979). TNW was supported in part by NIH training grant T32-HD007516.

REFERENCES

1. Lindvall, O, Kokaia, Z and Martinez-Serrano, A (2004). Stem cell therapy for human neurodegenerative disorders-how to make it work. *Nat Med* **10 Suppl**: S42–S50.
2. Müller, FJ, Snyder, EY and Loring, JF (2006). Gene therapy: can neural stem cells deliver? *Nat Rev Neurosci* **7**: 75–84.
3. Jeon, I, Lee, N, Li, JY, Park, IH, Park, KS, Moon, J *et al.* (2012). Neuronal properties, *in vivo* effects, and pathology of a Huntington's disease patient-derived induced pluripotent stem cells. *Stem Cells* **30**: 2054–2062.
4. Wernig, M, Meissner, A, Cassady, JP and Jaenisch, R (2008). c-Myc is dispensable for direct reprogramming of mouse fibroblasts. *Cell Stem Cell* **2**: 10–12.
5. Roy, NS, Cleren, C, Singh, SK, Yang, L, Beal, MF and Goldman, SA (2006). Functional engraftment of human ES cell-derived dopaminergic neurons enriched by coculture with telomerase-immortalized midbrain astrocytes. *Nat Med* **12**: 1259–1268.
6. Miura, K, Okada, Y, Aoi, T, Okada, A, Takahashi, K, Okita, K *et al.* (2009). Variation in the safety of induced pluripotent stem cell lines. *Nat Biotechnol* **27**: 743–745.
7. Koch, P, Opitz, T, Steinbeck, JA, Ladewig, J and Brüstle, O (2009). A rosette-type, self-renewing human ES cell-derived neural stem cell with potential for *in vitro* instruction and synaptic integration. *Proc Natl Acad Sci USA* **106**: 3225–3230.
8. Chaubey, S and Wolfe, JH (2013). Transplantation of CD15-enriched murine neural stem cells increases total engraftment and shifts differentiation toward the oligodendrocyte lineage. *Stem Cells Transl Med* **2**: 444–454.
9. Englund, U, Bjorklund, A, Wictorin, K, Lindvall, O and Kokaia, M (2002). Grafted neural stem cells develop into functional pyramidal neurons and integrate into host cortical circuitry. *Proc Natl Acad Sci USA* **99**: 17089–17094.
10. Alvarez-Dolado, M, Calcagnotto, ME, Karkar, KM, Southwell, DG, Jones-Davis, DM, Estrada, RC *et al.* (2006). Cortical inhibition modified by embryonic neural precursors grafted into the postnatal brain. *J Neurosci* **26**: 7380–7389.
11. Oki, K, Tatarishvili, J, Wood, J, Koch, P, Wattananit, S, Mine, Y *et al.* (2012). Human-induced pluripotent stem cells form functional neurons and improve recovery after grafting in stroke-damaged brain. *Stem Cells* **30**: 1120–1133.
12. Wernig, M, Benninger, F, Schmandt, T, Rade, M, Tucker, KL, Büssow, H *et al.* (2004). Functional integration of embryonic stem cell-derived neurons in vivo. *J Neurosci* **24**: 5258–5268.
13. Petersen, CC (2007). The functional organization of the barrel cortex. *Neuron* **56**: 339–355.
14. Carlson, GC and Coulter, DA (2008). *In vitro* functional imaging in brain slices using fast voltage-sensitive dye imaging combined with whole-cell patch recording. *Nat Protoc* **3**: 249–255.
15. Contreras, D and Llinas, R (2001). Voltage-sensitive dye imaging of neocortical spatiotemporal dynamics to afferent activation frequency. *J Neurosci* **21**: 9403–9413.
16. Cohen, LB and Salzberg, BM (1978). Optical measurement of membrane potential. *Rev Physiol Biochem Pharmacol* **83**: 35–88.
17. Ryder, EF, Snyder, EY and Cepko, CL (1990). Establishment and characterization of multipotent neural cell lines using retrovirus vector-mediated oncogene transfer. *J Neurobiol* **21**: 356–375.
18. Watson, DJ, Walton, RM, Magnitsky, SG, Bulte, JW, Poptani, H and Wolfe, JH (2006). Structure-specific patterns of neural stem cell engraftment after transplantation in the adult mouse brain. *Hum Gene Ther* **17**: 693–704.
19. Magnitsky, S, Walton, RM, Wolfe, JH and Poptani, H (2008). Magnetic resonance imaging detects differences in migration between primary and immortalized neural stem cells. *Acad Radiol* **15**: 1269–1281.
20. Demeter, K, Herberth, B, Duda, E, Domonkos, A, Jaffredo, T, Herman, JP *et al.* (2004). Fate of cloned embryonic neuroectodermal cells implanted into the adult, newborn and embryonic forebrain. *Exp Neurol* **188**: 254–267.
21. Lundberg, C, Englund, U, Trono, D, Björklund, A and Wictorin, K (2002). Differentiation of the RN33B cell line into forebrain projection neurons after transplantation into the neonatal rat brain. *Exp Neurol* **175**: 370–387.
22. Snyder, EY, Taylor, RM and Wolfe, JH (1995). Neural progenitor cell engraftment corrects lysosomal storage throughout the MPS VII mouse brain. *Nature* **374**: 367–370.
23. Flax, JD, Aurora, S, Yang, C, Simonin, C, Wills, AM, Billinghurst, LL *et al.* (1998). Engraftable human neural stem cells respond to developmental cues, replace neurons, and express foreign genes. *Nat Biotechnol* **16**: 1033–1039.
24. Park, KI, Teng, YD and Snyder, EY (2002). The injured brain interacts reciprocally with neural stem cells supported by scaffolds to reconstitute lost tissue. *Nat Biotechnol* **20**: 1111–1117.
25. Riess, P, Zhang, C, Saatman, KE, Laurer, HL, Longhi, LG, Raghupathi, R *et al.* (2002). Transplanted neural stem cells survive, differentiate, and improve neurological motor function after experimental traumatic brain injury. *Neurosurgery* **51**: 1043–52; discussion 1052.
26. Teng, YD, Lavik, EB, Qu, X, Park, KI, Ourednik, J, Zurakowski, D *et al.* (2002). Functional recovery following traumatic spinal cord injury mediated by a unique polymer scaffold seeded with neural stem cells. *Proc Natl Acad Sci USA* **99**: 3024–3029.
27. Wester, JC and Contreras, D (2012). Columnar interactions determine horizontal propagation of recurrent network activity in neocortex. *J Neurosci* **32**: 5454–5471.

28. Lefort, S, Tomm, C, Floyd Sarria, JC and Petersen, CC (2009). The excitatory neuronal network of the C2 barrel column in mouse primary somatosensory cortex. *Neuron* **61**: 301–316.
29. Civillico, EF and Contreras, D (2006). Integration of evoked responses in supragranular cortex studied with optical recordings in vivo. *J Neurophysiol* **96**: 336–351.
30. Petersen, CC and Sakmann, B (2001). Functionally independent columns of rat somatosensory barrel cortex revealed with voltage-sensitive dye imaging. *J Neurosci* **21**: 8435–8446.
31. Petersen, CC, Grinvald, A and Sakmann, B (2003). Spatiotemporal dynamics of sensory responses in layer 2/3 of rat barrel cortex measured *in vivo* by voltage-sensitive dye imaging combined with whole-cell voltage recordings and neuron reconstructions. *J Neurosci* **23**: 1298–1309.
32. Jäderstad, J, Jäderstad, LM, Li, J, Chintawar, S, Salto, C, Pandolfo, M *et al.* (2010). Communication via gap junctions underlies early functional and beneficial interactions between grafted neural stem cells and the host. *Proc Natl Acad Sci USA* **107**: 5184–5189.
33. Lo Turco, JJ and Kriegstein, AR (1991). Clusters of coupled neuroblasts in embryonic neocortex. *Science* **252**: 563–566.
34. Borgdorff, AJ, Poulet, JF and Petersen, CC (2007). Facilitating sensory responses in developing mouse somatosensory barrel cortex. *J Neurophysiol* **97**: 2992–3003.
35. Stevens, JR, Phillips, I, Freed, WJ and Poltorak, M (1988). Cerebral transplants for seizures: preliminary results. *Epilepsia* **29**: 731–737.
36. Baraban, SC, Southwell, DG, Estrada, RC, Jones, DL, Sebe, JY, Alfaro-Cervello, C *et al.* (2009). Reduction of seizures by transplantation of cortical GABAergic interneuron precursors into Kv1.1 mutant mice. *Proc Natl Acad Sci USA* **106**: 15472–15477.
37. Ortinski, PI, Dong, J, Mungenast, A, Yue, C, Takano, H, Watson, DJ *et al.* (2010). Selective induction of astrocytic gliosis generates deficits in neuronal inhibition. *Nat Neurosci* **13**: 584–591.
38. Pascual, O, Ben Achour, S, Rostaing, P, Triller, A and Bessis, A (2012). Microglia activation triggers astrocyte-mediated modulation of excitatory neurotransmission. *Proc Natl Acad Sci USA* **109**: E197–E205.
39. Ueno, M, Fujita, Y, Tanaka, T, Nakamura, Y, Kikuta, J, Ishii, M, *et al.* (2013). Layer V cortical neurons require microglial support for survival during postnatal development. *Nat. Neurosci.* doi:10.1038/nn.3358.
40. Ma, C, Greenquist, KW and Lamotte, RH (2006). Inflammatory mediators enhance the excitability of chronically compressed dorsal root ganglion neurons. *J Neurophysiol* **95**: 2098–2107.
41. Southwell, DG, Paredes, MF, Galvao, RP, Jones, DL, Froemke, RC, Sebe, JY *et al.* (2012). Intrinsically determined cell death of developing cortical interneurons. *Nature* **491**: 109–113.
42. Blaschke, AJ, Staley, K and Chun, J (1996). Widespread programmed cell death in proliferative and postmitotic regions of the fetal cerebral cortex. *Development* **122**: 1165–1174.
43. Pucilowska, J, Puzerey, PA, Karlo, JC, Galán, RF and Landreth, GE (2012). Disrupted ERK signaling during cortical development leads to abnormal progenitor proliferation, neuronal and network excitability and behavior, modeling human neuro-cardio-facial-cutaneous and related syndromes. *J Neurosci* **32**: 8663–8677.
44. Holmgren, C, Harkany, T, Svennenfors, B and Zilberter, Y (2003). Pyramidal cell communication within local networks in layer 2/3 of rat neocortex. *J Physiol (Lond)* **551**(Pt 1): 139–153.
45. Manns, ID, Sakmann, B and Brecht, M (2004). Sub- and suprathreshold receptive field properties of pyramidal neurones in layers 5A and 5B of rat somatosensory barrel cortex. *J Physiol (Lond)* **556**(Pt 2): 601–622.
46. Weick, JP, Liu, Y and Zhang, SC (2011). Human embryonic stem cell-derived neurons adopt and regulate the activity of an established neural network. *Proc Natl Acad Sci USA* **108**: 20189–20194.
47. Piña-Crespo, JC, Talantova, M, Cho, EG, Soussou, W, Dolatabadi, N, Ryan, SD *et al.* (2012). High-frequency hippocampal oscillations activated by optogenetic stimulation of transplanted human ESC-derived neurons. *J Neurosci* **32**: 15837–15842.
48. Nelson, PT, Kondziolka, D, Wechsler, L, Goldstein, S, Gebel, J, DeCesare, S *et al.* (2002). Clonal human (hNT) neuron grafts for stroke therapy: neuropathology in a patient 27 months after implantation. *Am J Pathol* **160**: 1201–1206.
49. Kondziolka, D, Steinberg, GK, Wechsler, L, Meltzer, CC, Elder, E, Gebel, J *et al.* (2005). Neurotransplantation for patients with subcortical motor stroke: a phase 2 randomized trial. *J Neurosurg* **103**: 38–45.
50. Taylor, RM and Wolfe, JH (1997). Decreased lysosomal storage in the adult MPS VII mouse brain in the vicinity of grafts of retroviral vector-corrected fibroblasts secreting high levels of beta-glucuronidase. *Nat Med* **3**: 771–774.
51. Peterka, DS, Takahashi, H and Yuste, R (2011). Imaging voltage in neurons. *Neuron* **69**: 9–21.
52. Nakai, J, Ohkura, M and Imoto, K (2001). A high signal-to-noise Ca(2+) probe composed of a single green fluorescent protein. *Nat Biotechnol* **19**: 137–141.
53. Schindelin, J, Arganda-Carreras, I, Frise, E, Kaynig, V, Longair, M, Pietzsch, T *et al.* (2012). Fiji: an open-source platform for biological-image analysis. *Nat Methods* **9**: 676–682.